Commun. Comput. Phys.
doi: 10.4208/cicp.021009.241210s

Vol. **9**, No. 5, pp. 1362-1374
May 2011

Mass Transport/Diffusion and Surface Reaction Process with Lattice Boltzmann

Giuseppe De Prisco[1,2,*] and Xiaowen Shan[1]

[1] *Exa Corporation, 55 Network Drive, Burlington, Massachusetts 01773, USA.*
[2] *Ingrain Inc, 3733 Westheimer Road, Houston, Texas 77027, USA.*

Received 2 October 2009; Accepted (in revised version) 24 December 2010

Available online 18 February 2011

Abstract. Multi-component flow with chemical reactions is a common problem in different industrial applications: the mixing chamber of a reaction injection molding (RIM) machine; the dynamics of diesel soot particles interacting with a porous-ceramic particulate filter; reactive transport in porous media; bio-chemical processes involving enzyme-catalyzed kinetics. In all these cases, mass diffusion/convection and wall or volume chemical interactions among components play an important role. In the present paper we underline the importance of diffusion/convection/reaction mechanisms in bio-chemical processes using the Lattice Boltzmann (LB) technique. The bio-application where we studied diffusion/convection/reaction mechanisms is the quorum-sensing pathway for the bio-synthesis of the AI-2, a molecule that allows the bacteria to launch a coordinated attack on a host immune system (see [9,10] for more details of the bio-application). The overall goal is to create a micro-device to screen potential drugs that inhibit AI-2 bio-synthesis. The Michaelis-Menten saturation kinetic model is implemented at the reactive surface and the results are shown in terms of two dimensionless numbers: Damkohler (*Da*) and Peclet (*Pe*) number. For high *Pe* number a small conversion of reactants into products is obtained at the reactive surface, but the overall flux of products is high; moreover, a fast saturation of the conversion of reactants to products is obtained for high *Da* numbers. The trade-off for setting the *Pe* and *Da* numbers depends on the specific application and the technologies used in the micro-device (e.g., sensitivity of the detector, cost of reactants).

AMS subject classifications: 76P05, 76R05, 76R50, 74F25, 92C45

PACS: 05.10.-a, 05.20.Dd, 47.11.Qr, 47.63.mf

Key words: Lattice Boltzmann, multi-component, diffusion-reaction.

*Corresponding author. *Email addresses:* deprisco@ingrainrocks.com (G. De Prisco), xiaowen@exa.com (X. Shan)

1 Introduction

Bio-sensors and bio-chips are one of the most useful and challenging application based on microfluidic devices for different kinds of problems like DNA analysis, protein separation, antibiotics screening [9, 10]. Using of microdevices is ideal for parallel and automatic drugs screening, and it allows using small volume of expensive reagents. The bio-application that we are focusing on in this paper, in order to study diffusion/convection/reaction mechanisms using Lattice Boltzmann technique, is the quorum-sensing pathway for the bio-synthesis of the AI-2, a molecule that allows the bacteria launching a coordinate attack on a host immune system. The overall goal is to create and to optimize a microdevice to screen potential drugs that inhibit the AI-2 bio-synthesis (see [9, 10] for more details).

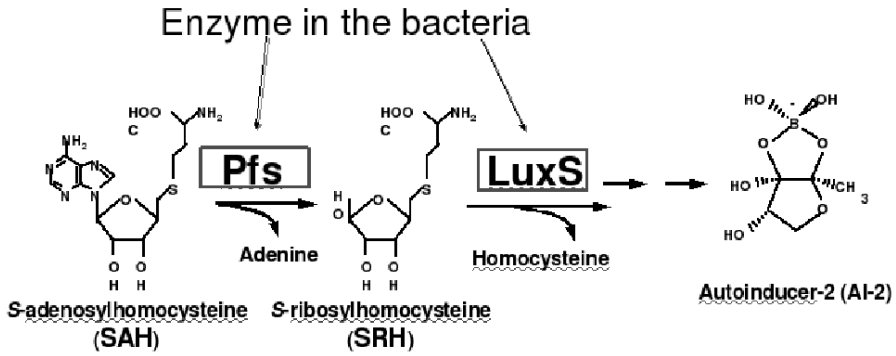

Figure 1: Schematic representation of the quorum sensing pathway (figure from [9,10]): the complex molecular SAH reacts with the enzyme Pfs giving adenine and SRH as product. The SRH reacts with the enzyme LuxS giving the by-product homocysteine and the autoinducer-2 (AI-2) (see [9, 10] for more details).

The quorum sensing pathway involve two kinds of enzymes: either the Pfs or LuxS (see Fig. 1). It is clear from the scheme in Fig. 1 that one mole of SAH that reacts with the enzyme Pfs gives one mole of adenine and one mole of SRH. The by-product adenine is not involved in the successive steps of the reaction, so a common simplification is to consider a reaction where one mole of SAH produces one mole of SRH. A microdevice that can mimic the quorum sensing pathway is a microchannel with two patches on the bottom surface. The enzymes Pfs and Luxs are attached on the surface of the patches with a fixed superficial concentration so that the two patches can be considered as reactive surfaces: when a molecule of a reactant reaches the surface of the patch it can react with the attached enzyme to generate a molecule of product. At the inlet of the microchannel is introduced a potential inhibitors of the AI-2 whose efficiency is analyzed through the microdevice [9,10]. A scheme of the microdevice is shown in Fig. 2; Fig. 3 shows the microchannel used in the experiment [9,10]. In order to optimize the microdevice in terms of maximum sensitivity, minimal sample requirement and fastest screening times, the quorum-sensing pathway was simulated with a LB code, and the results were compared with available experimental analysis [9, 10]. The experimental analysis [9, 10] was con-

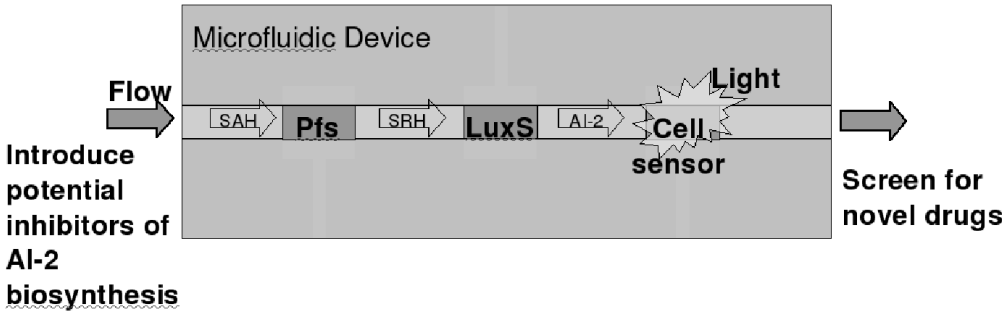

Figure 2: Schematic representation of the microchannel with reactive patch to mimic the quorum sensing pathway (figure from [9, 10]); on the reactive patch are attached the enzymes Pfs and LuxS. At the inlet of the channel, potential inhibitors of the AI-2 are introduced. Those inhibitors are injected with a transporting background flow that can be water. At the end of the microchannel a light sensor can detect the presence of the AI-2 autoinducer (see [9, 10] for more details).

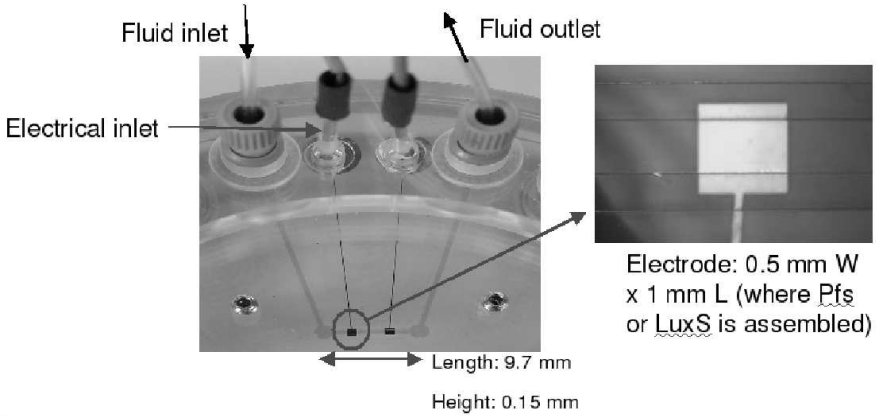

Figure 3: The blue tiny line is the microchannel used in the experiment [9, 10]. Figure from [9, 10].

ducted for one of the two steps of the quorum-sensing pathway (the reaction of the SAH to produce the SRH molecule), so the simulations were conducted for the same reaction. In this study the authors proved that this numerical technique is able to reproduce the correct trend in convection-diffusion-reaction processes, and it allows to optimizing the microdevice with a short turnaround time.

2 Multi-components lattice Boltzmann model

The lattice Boltzmann method [1, 17] is a kinetic theory based method that recovers the Navier-Stokes hydrodynamics at the macroscopic level while maintaining a kinetic picture in the simulation. The kinetic nature of the method allows the reaction physics to be modeled more intuitively both at the boundaries and in the bulk of the fluid. In the present work, we model the problem of convection-diffusion of the reactants and prod-

ucts and the surface reaction for the biosynthesis of the AI-2 using the previously proposed multi-component LB method [11–14] in which, each of the components is represented by its own distribution function. Here we only very briefly review the key points of the multi-component LB model used in the present study, and readers are referred to the aforementioned references for more details.

Let $f_\sigma(\boldsymbol{x},\boldsymbol{\xi},t)$ be the distribution function of the σ-th component in the phase space of $(\boldsymbol{x},\boldsymbol{\xi})$ at time t. As shown previously [15, 16], the BGK equation can be discretized in velocity space using a small set of discrete velocities $\{\boldsymbol{\xi}_a : a=1,\cdots,d\}$. Noting $f_a^\sigma(\boldsymbol{x},t) = f_\sigma(\boldsymbol{x},\boldsymbol{\xi}_a,t)$, f_a^σ satisfies the following multi-component lattice BGK equation:

$$f_a^\sigma(\boldsymbol{x}+\boldsymbol{\xi}_a,t+1)-f_a^\sigma(\boldsymbol{x},t)=-\frac{1}{\tau_\sigma}\left[f_a^\sigma-f_a^{\sigma(eq)}\right], \qquad \sigma=1,\cdots,S, \tag{2.1}$$

where τ_σ is the relaxation time of the σ-th component and S the total number of components.

In addition, to model the interactions among particles of different species, an interaction force is introduced between particles on neighboring sites. Specifically, the force on particles of component σ at site $\boldsymbol{x}$ is:

$$\boldsymbol{F}_\sigma(\boldsymbol{x})=-\psi_\sigma(\boldsymbol{x})\sum_{\varsigma=1}^{S}G_{\sigma\varsigma}\sum_{a=1}^{d}\psi_\varsigma(\boldsymbol{x}+\boldsymbol{e}_a)\boldsymbol{e}_a, \tag{2.2}$$

where ψ_σ is a pseudo-potential of the σ-th component, $\boldsymbol{e}_a$ the vectors pointing from $\boldsymbol{x}$ to its d interacting neighbors, and $G_{\sigma\varsigma}$ a Green's function regulating the interaction strength between different components. The interaction force enters into the LB dynamics of Eq. (2.1) either through a simple increment of momentum in the equilibrium distribution function [11], or in a more accurate treatment, through a modified collision term [3]. As shown previously in [13, 14], the inter-molecular interaction changes the mutual diffusivities independent of the viscosity, and we point out here that the large variation of the diffusivities observed in liquids are physically due to the inter-molecular interactions. The only physically consistent way of modeling the large variation in diffusivity is through the modeling of the inter-molecular interactions.

3 Enzyme binding kinetic model

Through the Chapman-Enskog expansion it can be proved that the discretize LB equation for the bulk flow recovers the correct continuity and momentum equations at the Navier-Stokes level. At the incompressible limit that we are interested in the present study, they are:

$$\frac{d\rho}{dt}=0 \qquad \text{and} \qquad \rho\frac{d\boldsymbol{u}}{dt}=-p+\mu\nabla^2\boldsymbol{u}, \tag{3.1}$$

where ρ is the total density, $\boldsymbol{u}$ the velocity, p the pressure, $d/dt \equiv \partial/\partial t+\boldsymbol{u}\cdot\nabla$, and μ the dynamic viscosity. The discretized LB equation for the solute (Reactants and Products)

recovers the correct convection-diffusion equations. The mathematical model that describes convection/diffusion/reaction within a volume can be summarized in the following system (see [2,4,18] for more details):

$$\frac{\partial C_i}{\partial t} = -\nabla \boldsymbol{N}_i + R_{i,V}, \tag{3.2a}$$

$$\boldsymbol{N}_i = -D_i \nabla C_i + \boldsymbol{u} C_i, \tag{3.2b}$$

where C_i is the volume concentration of the specie i, D_i is its diffusivity and $R_{i,V}$ account for the reaction rate within the volume, so it can be a rate of creation or consumption of the specie i. $\boldsymbol{N}_i$ is the molar flux of the specie i. In the present paper one mole of a reactant gives one mole of product and molar flux and mass flux are equivalent. Moreover, there is no reaction rate in the volume, so the term R_i is zero. On the other hand, a chemical reaction is defined on the wall so appropriate model should be accounted for the surface adsorption/blowing of the flux of one or more species. The following model is typically used [2,4,18] for the bio-catalyzed kinetics:

$$\frac{d[P]}{dt} = k_2[RE], \tag{3.3a}$$

$$\frac{d[RE]}{dt} = k_1[R][E] - (k_{-1} + k_2)[RE], \tag{3.3b}$$

$$[E] = [E]_0 - [RE]. \tag{3.3c}$$

Eqs. (3.3a)-(3.3c) are the reversible kinetic reaction at the solid-fluid interface of reactants, $[R]$, and products, $[P]$, through the complex, $[RE]$, both soluble in the bulk fluid. The reaction model is implemented as boundary condition on the wall (reactive surface): the mass transfer of reactants to the reactive surface and of the products away from the wall is addressed by Eqs. (3.3a)-(3.3c). Others models used to analyzed similar surface reactions are also possible: for example, for the simulation of dissolution and precipitation in porous media the reader can read [5–8].

It is important to understand how the enzyme kinetic works to choose the appropriate boundary condition on the wall. The enzyme-catalyzed production of a product $[P]$ from a reactant $[R]$ involves two steps: the reactant that is in physical contact with the enzyme is bound by the enzyme to form an enzyme-reactant complex ($[RE]$). After the binding, either the product $[P]$ is formed or the complex $[RE]$ goes back to the original dissociated form $[R]+[E]$. Those steps are summarized in the previous Eqs. (3.3a)-(3.3c), where the first two equations are the rate of products formation, and the rate of variation of the complex $[RE]$, and the last equation is the conservation equation of enzyme, where $[E]_0$ is the initial superficial concentration. The total concentration of enzyme $[E]_0$ is fixed but the concentration available each time to bind new reactant $[E]$ depends on the free sites that are not linked yet with a reactant. k_1 is the rate of the association of reactant and enzyme; k_{-1} is the rate of dissociation of unaltered substrate from the enzyme; k_2 is the rate of dissociation of product from the enzyme. The variation of the complex $[RE]$ is zero

in the hypothesis of steady state; in this hypothesis the $[RE]$ complex is being formed and broken at the same rate and the Michealis-Menten saturation kinetic can be easily derived from the previous equation:

$$[\dot{P}] = \frac{[R]}{K_M + [R]} k_2 [E]_0, \tag{3.4a}$$

$$K_M = \frac{k_2 + k_{-1}}{k_1}. \tag{3.4b}$$

The product $[E]_0 k_2$ is the maximum rate that can be achieved when all the enzyme molecules have reactants bound. K_M is the Michaelis constant that represents the reactant concentration at which the reaction occur at half of the maximum rate.

To summarize, in the LB based code the amount of products injected at each time step from the patch in to the volume is modulated by the Michaelis-Menten saturation kinetic, in particular by the product $[E]_0 k_2$. The evolution of a generic solute C_i in the bulk flow with average velocity $\boldsymbol{u}$ is governed by the convection-diffusion Eq. (3.2). Eq. (3.4) is a boundary condition that account for the mass transfer of one solute in another at the surface. Eq. (3.2) are never implemented directly in the numerical code but they are recovered with the LB equation (paragraph 2). The Eq. (3.4), instead, is implemented directly as boundary condition, in particular for the evaluation of the equilibrium distribution at the wall, so it acts in concert with the Eq. (3.2).

3.1 LB model of the enzyme binding kinetic and simulation set-up

The simulation model for the microchannel is a channel with height h and width w with $h \ll w$ so that the problem is simplified to a 2D problem. It is useful to consider the dimensionless equations. The scaled equations are:

$$\frac{\partial C_i^*}{\partial \tau} = \nabla^{*2} C_i^* - Pe \boldsymbol{u} \nabla^* C_i^*, \tag{3.5a}$$

$$\frac{\partial C_P^*}{\partial \tau}\Big|_{Patch} = \epsilon Da^{II} \frac{C_{i,Patch}^*}{K_M^* + C_{i,Patch}^*}, \tag{3.5b}$$

with the dimensionless parameters been: $x^* = x/h$, $y^* = y/h$, $\tau = Dt/h2$, $C_i^* = C_i / C_{R,x=0}$, $C_{i,patch} = C_{i,patch}/(C_i h)$, $K_M^* = K_M / C_{R,x=0}$, $\boldsymbol{u}^* = \boldsymbol{u}/U$, where U is the averaged velocity, D is the diffusion of the reactant in water that is the background convection fluid. $C_{R,x=0}$ is the reference concentration of the reactants at the inlet of the microchannel $x = 0$. $Pe = Uh/D$ is the Peclet number that can be interpreted as the ratio between the diffusion time and the convection time. $Da^{II} = h^2 k/D$ is the second Damkohler number that is the ratio between diffusion and reaction time. $\epsilon = E0/(hC_{R,x=0})$ is the relative density of enzyme-reactant at the surface, so it represents the absorption capacity of the surface, and it is fixed in the simulation as in the experiments (0.33). A geometrical parameter that influences the production rate, is the aspect ratio between the channel height and the length

of the surface where the Michaelis-Menten saturation kinetic is applied; the aspect ratio in the present case is 6.7. The concentration of the reactant is also specified with respect to the background material: the ratio between the two species is fixed as in the experiments, 55×10^3. The value of the Michaelis constant K_M was fixed trough the equilibrium dissociation constant in the experiment, $K_D=K_M/C_{R,x=0}=0.12$. The value of the velocity is chosen large enough to have a short transient, but small enough to have inertial effect negligible as in the experiment (approximation of the Stokes flow). In the following numerical simulations, the *Re* number is order of 1; in the experiment Reynolds number is order of 0.1. Because the reactants and the products are very dilutes in the background species (water), and they are treated as perfect gas (no interaction is considered among the different species, so that $G_{ij}=0$ in the LB code), the diffusivity of each species can be approximated with their viscosity in the LB code [13]. The diffusivity is obtained from the Peclet number, with two limitations: that it has to be no lower than 0.01 for stability reason (this gives the maximum simulated *Pe* for a specific average velocity of the bulk flow and aspect ratio), and that the diffusivity of each species must be much smaller than the viscosity of the background species. In other words, Schmidt number (*Sc*) never exceeds 1000. For example, if the $Pe=230$, the viscosity of the reactant and product was fixed to 0.015 and the viscosity of the background to 0.4. Different Peclet numbers are obtained changing the pressure drop inlet-outlet, so the flow rate. The averaged velocity, was never higher than 0.11 to avoid compressibility effects. The rate of dissociation of products from the enzyme k_2 was obtained from the Damkohler number, so different Damkohler numbers are obtained changing the k_2 constant. The maximum *Da* number analyzed is fixed through the maximum k_2 for a specific aspect ratio and diffusivity. The dissociation constant k_2 directly influences the equilibrium distribution calculation of the reactant and product at the reactive patch. The limitation on the value of the constant k_2 (more exactly for the product $k_2[E]_0$) is that k_2 must be much smaller than the initial concentration of the reactant at the wall; in the case this condition is not verified, the concentration of reactants can become negative at the wall after the first time step. The total number of binding sites $[E]_0$ are obtained from the parameter epsilon known in the experiment (=0.33); the binding sites $[E]_0$ are never changed because the aspect ratio and the inlet concentration of the reactant is fixed. For each time step, the equilibrium distribution of the reactant and product at the reactive patch was adjusted according to the boundary condition imposed by the Michaelis-Menten kinetic. The number of lattice points are 600 in the streamwise direction x and 40 in the normal direction y. The reactive patch is centered in the middle of the bottom surface of the channel. The other walls are treated with a no-slip boundary condition. At the inflow the ratio between concentration of reactant and the concentration of the background fluid is assigned according to the experimental value. Homogeneous Neumann boundary conditions are applied for the velocity vector at the inlet and outlet. The flow is pressure driven. At the inlet the bulk and reactants concentration is fixed (the ratio is fixed through the experiments). The density (pressure) of the bulk flow is fixed in a way to have a *Re* number in the order of 1. The pressure drop between inlet and outlet is established with the following condition

on the outlet concentrations:

$$C_i = \frac{C_{i,bc}(C_{i,x=0} - \Delta P)}{\sum_i C_{i,bc}}, \tag{3.6}$$

where $C_{i,bc}$ is the concentration at the outlet before collision. The condition (3.4) makes sure that the total mass of the species is conserved. Moreover, each species at the outlet is only convected out by the flow, so no diffusion is considered ($C_i/x = 0$). On the reactive surface, the distribution of particles is updated with the Michaelis-Menten saturation kinetic, so on each time step the equilibrium distribution of the reactants and the products is updated with the number of particle obtained by Eq. (3.4).

4 Results and discussion

The results are parameterized in term of Pe and Da numbers. The steady state velocity profile matches very well the analytical Poiseuille flow. Fig. 4 shows the percentage of conversion of reactants in to products as a function of Pe number and Da fixed to 52. The percentage of conversion is defined as

$$\%\text{Conversion} = \frac{(\Phi_{input} - \Phi_{output})}{\Phi_{input}}, \tag{4.1}$$

where Φ is the mass flux of the reactant. The percentage of conversion increases with decreasing the Pe number (that is equivalent of changing the averaged flow velocity keeping the other parameters fixed). This is expected because for small Pe numbers, the diffusion mechanism is predominant so a reactant has more time to reach the reactive patch. At the same time, however, the time required to convert a specific amount of reactant in product increases; for example, for zero mass flux ($Pe = 0$), all the reactants will be converted in to products in an infinite time because fresh reactants are transported only by diffusion on the reactive patch (Fig. 4). In this case the process is diffusion limited. Increasing Pe gives an increase of the conversion rate (Fig. 5), but the percentage of conversion with respect to the fresh reactants available at the inlet decreases (Fig. 4) because the diffusion process becomes negligible: with an high enough Pe, a solute in the bulk flow has less time to diffuse up to the reactive patch, so the overall conversion rate decreases until becomes constant for high Pe. In this case, the diffusion does not affect the transport of solute and the concentration of particle close to the reactive surface is only fixed by the averaged velocity of the bulk fluid; in other terms, more reactants at the inlet are wasted increasing Pe (in the sense that do not react), and the mass of reactant that converts in to product becomes a small percentage of the reactant available at the inlet. In this case, the conversion process is limited by the velocity of the reaction and the aspect ratio. It is easy to extrapolate that with a channel high enough, this percentage will tend to zero increasing Pe so that almost all the reactants will be transported without reaching the reactive surface. Note that conversion rate is maximized at the extremes of the patch, where the diffusion process supplies fresh reactant from a wider angle of

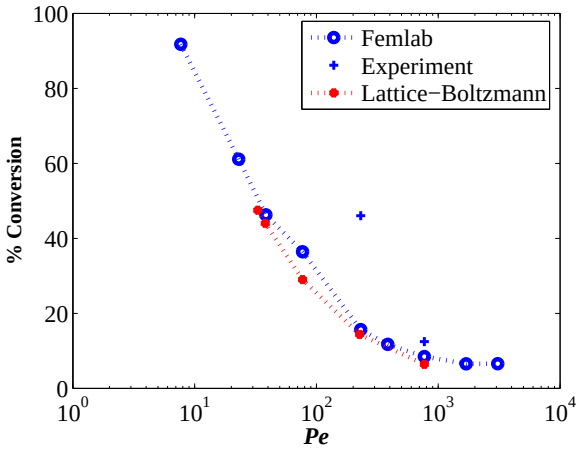

Figure 4: Conversion of the reactants in products as function of the Pe, and Da fixed to 52. For small Pe all the reactants are converted in to products, but in an infinite time because fresh reactants are transported only by diffusion on the reactive patch (reaction and Diffusion limited). For high Pe number the amount of particles that can be exchanged at the reactive patch is limited by the saturation kinetics of Michaelis-Menten and the length of the reactive patch, so the conversion becomes reaction and aspect ratio limited. In this condition, the percentage of conversion can be changed only changing the Da number. See [9, 10] for further discussion of experimental and Femlab results.

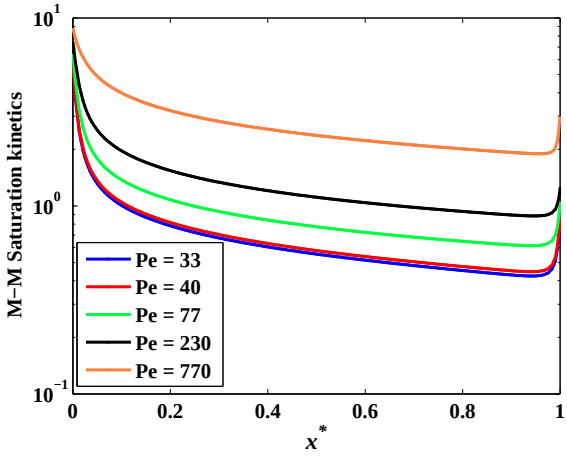

Figure 5: Production of the new species at the wall (Da fixed to 52). The x axis is normalized so that $x=0$ is at the beginning of the reactive patch and $x=1$ is at the end.The total dimensionless production rate of product (Michaelis-Menton kinetic) is reported in the y axis. The conversion rate increases with Pe and is maximized at the extremes of the patch, where the diffusion process supplies fresh reactant from a wider angle of directions so the reaction rate is maximized. Moreover, the fresh reactants are reacting along the patch in the direction of the bulk flow, so the reaction rate decreases along the same patch.

directions so the reaction rate is maximized. Moreover, the fresh reactants are reacting along the patch in the direction of the bulk flow, so the reaction rate decreases along the same patch (Fig. 5). The previous analysis is quantified in Figs. 4 and 5 and agrees very well with the trend reported in [5].

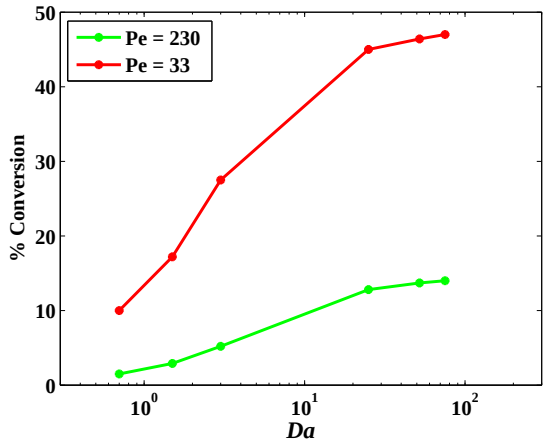

Figure 6: Conversion of the reactants in products as function of the Da number.

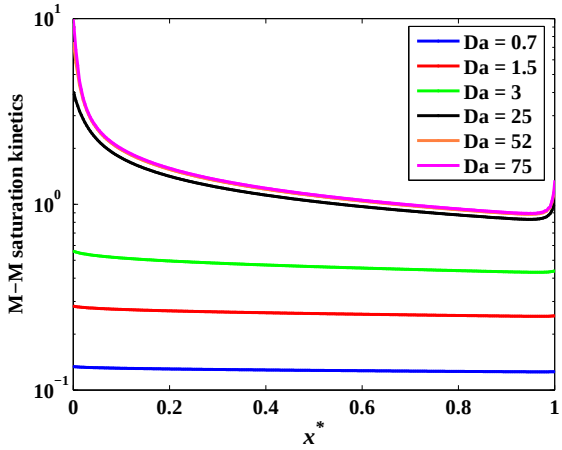

Figure 7: Production of the new species at the wall (Pe fixed to 230). The x axis is normalized so that $x=0$ is at the beginning of the reactive patch and $x=1$ is at the end. On the y axis there is the total dimensionless production rate of product that is the Michaelis-Menton kinetic.

The variation of the percentage of conversion as a function of Da number is shown in Fig. 6 for two different Pe numbers. For small Da the conversion is also small, and the consumption of reactants for time step is small as well, as it is shown in Figs. 7 ($Pe=230$) and 8 ($Pe=33$). In this case, the production of the new species can be considered as reaction limited: the reaction time is longer than the diffusion and convection time; in fact, as it is shown in Figs. 7 and 8, the production rate is constant over the whole reactive patch and does not change with the Pe number. As the Da number increases, the conversion increases proportionally because a higher number of particles have time to be converted on the reactive patch. For Da number high enough, the conversion and the production of particle per unit of time becomes transported limited (the reaction time is so small that does not have an influence in the conversion) so that the two mechanisms

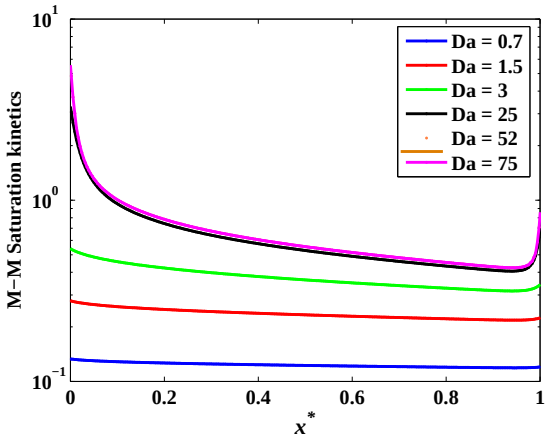

Figure 8: Production of the new species at the wall (Pe fixed to 33). The x axis is normalized so that $x=0$ is at the beginning of the reactive patch and $x=1$ is at the end. On the y axis there is the total dimensionless production rate of product that is the Michaelis-Menton kinetic.

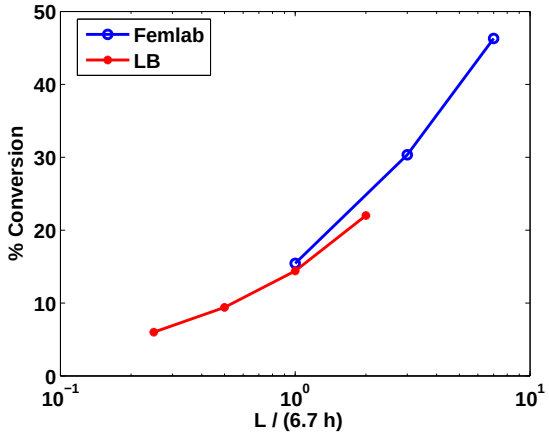

Figure 9: Conversion of the reactants in products as function of the aspect ratio ($Pe=230$ and $Da=52$).

of convection and diffusion are in competition. In Fig. 9 is presented the variation of percentage of conversion as a function of the aspect ratio, with Pe fixed to 230 and Da to 52. If the height of the channel is fixed, higher conversion is obtained for longer patch. The results agree with the results in [9,10] and in [5].

5 Conclusions and future works

The results show that for high Pe number a small percentage of conversion of reactants in to products is obtained, but the total amount of products within a fixed amount of time increases; this means that a high amount of reactant is wasted for high Pe numbers, but a high molar flux is exchanged at interactive patch. As the Da number increases, the

conversion increases proportionally. The trade-off depends on the specific application and overall goal. If, for example, the interactive patch is in a device that works only if the number of particle per time is above a certain threshold, high flow rate could be beneficial. On the other hand, if the reactants are expensive, the goal could be to work close to the transport limited region in order to minimize the wasted reactant. An extension of this work that can be obtained easily with LB method is to evaluate the variation of the Reactant-Product complex ([RE]) as function of Pe and Da numbers. In order to do this a first order liner differential equation needed to be solved each time step so that the hypothesis of steady state is not needed. This can be an interesting steps because, within the authors knowledge, is not possible measure the variation of this complex experimentally because its dynamic is too fast. It is also possible to validate the Michaelis-Menton kinetic approximation for different kinds of enzymes. We thank Dr. Angela Lewandowski and Bentley Research Group at University of Maryland for helpful discussion, for using their images and results.

References

[1] S. Chen and G. Doolen, Lattice Boltzmann method for fluid flows, Ann. Rev. Fluid. Mech., 30 (1998), 329–364.
[2] T. Gervais and K. F. Jensen, Mass transport and surface reactions in microfluidic systems, Chem. Eng. Sci., 61(4) (2006), 1102–1121.
[3] Z. Guo, C. Zheng and B. Shi, Discrete lattice effects on the forcing term in the lattice Boltzmann method, Phys. Rev. E., 65 (2002), 046308.
[4] G. Hu, Y. Gao and D. Li, Modeling micropatterned antigen-antibody binding kinetics in a microfluidic chip, Biosens. Bioelectron., 22(7) (2007), 1403–1409.
[5] Q. Kang, P. C. Lichtner and D. Zhang, Lattice Boltzmann pore-scale model for multicomponent reactive transport in porous media, J. Geophys. Res., 111 (2006), B05203.
[6] Q. Kang, P. C. Lichtner and D. Zhang, An improved lattice Boltzmann model for multicomponent reactive transport in porous media at the pore scale, Water. Resour. Res., 43 (2007), W12S14.
[7] Q. Kang, D. Zhang and S. Chen, Simulation of dissolution and precipitation in porous media, J. Geophys. Res., 108(B10) (2003), 2505–2513.
[8] Q. Kang, D. Zhang, S. Chen and X. He, Lattice Boltzmann simulation of chemical dissolution in porous media, Phys. Rev. E., 65 (2002), 036318.
[9] A. T. Lewandowski, Assembly of Quorum Sensing Pathway Enzymes onto Patterned Microfabricated Devices, PhD thesis, University of Maryland, College Park, 2007.
[10] X. L. Luo, Programmable Biomolecule Assembly and Activity in Prepackaged BioMEMS, PhD thesis, University of Maryland, College Park, 2008.
[11] X. Shan and H. Chen, Lattice Boltzmann model for simulating flows with multiple phases and components, Phys. Rev. E., 47(3) (1993), 1815–1819.
[12] X. Shan and H. Chen, Simulation of non-ideal gases and liquid-gas phase transitions by lattice Boltzmann equation, Phys. Rev. E., 49(4) (1994), 2941–2948.
[13] X. Shan and G. Doolen, Multi-component lattice Boltzmann model with interparticle interaction, J. Stat. Phys., 81 (1995), 379–393.

[14] X. Shan and G. Doolen, Diffusion in a multi-component lattice Boltzmann equation model, Phys. Rev. E., 54(4) (1996), 3614–3620.
[15] X. Shan and X. He, Discretization of the velocity space in solution of the Boltzmann equation, Phys. Rev. Lett., 80 (1998), 65–68.
[16] X. Shan, X.-F. Yuan and H. Chen, Kinetic theory representation of hydrodynamics: a way beyond the Navier-Stokes equation, J. Fluid. Mech., 550 (2006), 413–441.
[17] S. Succi, The Lattice Boltzmann Equation for Fluid Dynamics and Beyond, Numerical Mathematics and Scientific Computation, Oxford University Press, 2001.
[18] M. Zimmermann, E. Delamarche, M. Wolf and P. Hunziker, Modeling and optimization of high-sensitivity, low-volume microfluidic-based surface immunoassays, Biomed. Microdevices., 7 (2005), 99–110.